





Digital Europe Programme Project **QCI-CAT**
QCI: Proof of Concept – Secure Connectivity Austria
Digital Europe Work Programme 2021-2022
EU Secure Quantum Communication Infrastructure (DIGITAL-2021-QCI-01)
Project number: 101091642

Project starting date: fixed date: 1 January 2023
Project end date: 31 March 2026
Project duration: 39 months

Document:	**Deliverable**
Type:	Demonstration
Dissemination Level:	Public
Title:	**Prototype of the UIBK Quantum Repeater**
Work-Package	WP8
Document number:	**D8.1**
Document Owner:	UIBK / Ben Lanyon
Contributors:	Ben Lanyon, Tracy Northup
Abstract:	A prototype quantum network was developed across the city of Innsbruck, consisting of three nodes: two trapped-ion systems within the same lab and a remote photon detection system connected by 17 km of commercial telecom optical fiber. The network and its components were used to demonstrate key aspects of a long-distance quantum repeater.



Key words:	Quantum Repeater, Trapped ions, Entanglement, Quantum Memory
Pages	26
Delivery Date Planned	2026-03-31 (M39)

Revision History

Version	Revision Points	Author(s) & Organization	Date
V 1.0	Initial version	Ben Lanyon (UIBK)	2026-02-04
V 1.1	Refined version	Ben Lanyon (UIBK)	2026-03-16
V 1.2	Proofreading / minor corrections	Tracy Northup (UIBK)	2026-03-17
V 1.3	Review-inspired corrections	Ben Lanyon (UIBK)	2026-03-20

Author List

Organization	Name	E-Mail address
UIBK	Ben Lanyon	Ben.lanyon@uibk.ac.at
UIBK	Tracy Northup	Tracy.northup@uibk.ac.at

Reviewer List

Organization	Name	E-Mail address
AIT	Marie-Christine Slater	Marie-christine.slater@ait.ac.at

Copyright Statement

The work described in this document has been conducted within the QCI-CAT project. This document reflects only the QCI-CAT Consortium view, and the European Union is not responsible for any use that may be made of the information it contains. This document and its content are the property of the QCI-CAT Consortium. All rights relevant to this document are determined by the applicable laws. Access to this document does not grant any right or license on the document or its contents. This document or its contents are not to be used or treated in any manner inconsistent with the rights or interests of the QCI-CAT Consortium or the Partners detriment and are not to be disclosed externally without prior written consent from the QCI-CAT Partners. Each QCI-CAT Partner may use this document in conformity with the QCI-CAT Consortium Grant Agreement provisions.

Funding Acknowledgement:

This project has received funding from the European Union's Digital Europe Work Programme 2021-2022 under Project number 101091642 and the National Foundation for Research, Technology and Development.

Table of content

Revision History 3
Author List 3
Reviewer List 3
Copyright Statement 3
Funding Acknowledgement: 3
List of Figures 4
List of Tables 4
Executive Summary 5
1. Introduction 6
1.1. Purpose and scope of the document 6
1.2. Target Audience 6
1.3. Relation to other project work 6
1.4. Structure of the document 6
2. Overview of our network and basic principles 7
3. Development of the repeater-node ion trap, 17 km fiber link and remote photon detection station 8
3.1. Repeater ion trap development 8
3.2. Deployed fibers and remote detection station development 9
4. Demonstration of a distributed quantum-repeater node 9
5. Development of a deployable ion-trap repeater node 10
6. Towards linking the two ion traps 11
Summary 13
Appendix A - List of Acronyms 14
Appendix B – Paper draft 15
Appendix C – Bibliography 26

List of Figures

Figure 1. **The developed three-node network.** 7
Figure 2. **The developed deployable ion-trap repeater node.** 11
Figure 3. **Schematic of the established experimental setup** 13

List of Tables

Table 1 List of Acronyms 14

Executive Summary

A three-node quantum network was developed, including a fiber link distributed across the city of Innsbruck, and then used to demonstrate key aspects of a long-distance quantum repeater node. In parallel, several significant advances were made in quantum repeater technology based on trapped atomic ions. Those developments include the development of a compact rack-mounted repeater node based on an ion-trap system for future data-centre deployment. This work completes deliverable D8.1 with the name 'Prototype of the UIBK Quantum Repeater'. This report outlines the key results and points to key subsequent scientific publications.

1. Introduction

The deliverable presented in this document is the culmination of the work done in **Task 8.1**, led by UIBK. That task focuses on the development of future quantum repeater technology based on trapped-ion systems. Specifically, we aimed to develop a quantum network made of three nodes: A, B and C, and to demonstrate key aspects of a long-distance quantum repeater. Nodes A and B are trapped-ion systems, connected by optical fiber and located in a laboratory on the University of Innsbruck campus. Node C is a photon detection station, connected via 17 kilometers of commercial telecom optical fiber that is deployed across the city of Innsbruck.

The associated deliverable **D 8.1** has the name 'Prototype of the UIBK Quantum Repeater', is of the type 'Demonstrator/prototype' and the specified format of the deliverable is 'Prototype and publication'.

1.1. Purpose and scope of the document

The purpose of the document is to present the Innsbruck prototype quantum repeater developments realised within the QCI-CAT project and provide links to, and drafts of, the associated research publications. At the time of writing this document, there are three weeks of work left in the QCI-CAT project and there is significant ongoing work, as shortly described towards the end of this document. The information in this document is up to date as of 11.03.2026.

1.2. Target Audience

The target audience for this document includes the EU review panel, the QCI-CAT internal reviewers as well as anyone from the general public with a scientific background.

1.3. Relation to other project work

Much of the QCI-CAT project is devoted to the development, deployment and demonstration of Quantum Key Distribution (QKD) protocols that exclusively use light and light detectors to distribute secure keys across optical fiber-based networks. Such schemes are typically limited to key distribution over fiber distances of maximally a few hundred kilometers. To extend these distances, at the expense of unconditional security, Task 8.4. saw the development of secure 'Trusted Nodes'. Quantum repeaters offer an unconditionally secure solution to enable key distribution over fiber-based networks of arbitrary distance. The principal functionalities of quantum repeaters are currently being developed in research laboratories around the world. Task 8.1 and associated deliverable D 8.1 represents QCI-CAT's efforts to develop and deploy quantum repeater technology based on trapped-ion systems.

1.4. Structure of the document

The next section (Section 2) presents an overview of the three-node network in the city of Innsbruck that has been developed for the QCI-CAT project, introducing the names of key elements and their desired functionalities. Section 3 presents key results in the development of a repeater-node ion trap and in the establishment of a long-distance fiber network and a remote photon detection station. Section 3 also includes references to four published documents that each present project results: two master's theses and two peer-reviewed research papers published in leading journals in the field of physics. Those references, and all others, are listed at the end of this document. Section 4 summarises the demonstration of a distributed repeater node using the new network. That section refers to a current draft of our research paper presenting those results; the draft is found in Appendix B and is currently being prepared for submission at project end (31.03.2026). Section 5 summarises our development of the second promised ion-trap network node (A), which is designed to be deployable in future in the sense that it can eventually be moved out of lab and into a data centre. Finally, Section 6 presents a status update on our present work to connect (entangle) the two ion-trap nodes in the QCI-CAT network.

2. Overview of our network and basic principles

The quantum network that we developed consists of three nodes: A, B and C. Nodes A and B are both trapped-ion systems, each capable of storing and manipulating quantum information encoded in atomic ions. Node C is a ***'remote photon detection station'***, capable of analysing and detecting quantum information encoded into the polarisation of single 1550 nm photons. The nodes are connected with optical fibers according to the linear geometry shown in Figure 1 below. The central node B is henceforth referred to as the '***repeater ion trap***' and the left node A is henceforth referred to as the '***deployable ion trap***'. The two ion traps are located in the same laboratory in Innsbruck, at the University of Innsbruck, and are linked by a few tens of meters of optical fiber. The remote photon detection station is in a village (industrial estate) located outside of Innsbruck, connected by two **co-propagating deployed optical fibers**: each 17 km long commercial telecom-wavelength SMF28 optical fibers, which traverse and exit the city.

The role of the central **repeater ion trap** (B) is to act as a quantum repeater node: to first establish entanglement between itself and with each of its neighbouring nodes via travelling photons (A-B and B-C) and then to swap the entanglement such that those nodes are directly entangled with one another (A-C). Entanglement between neighbouring nodes is established via the distribution of ion-entangled photons through the optical fibers. Ion-entangled photons are generated by each ion-trap node via a cavity-mediated Raman process [Stute12], triggered via a laser pulse. A key feature of the repeater node is that it contains multiple ions and is capable of performing universal quantum information processing operations.

Before the QCI-CAT project began, the only element of the network that existed was the repeater-node ion trap. All the rest of the network was developed, tested and used during the QCI-CAT project, as now described in the coming sections.

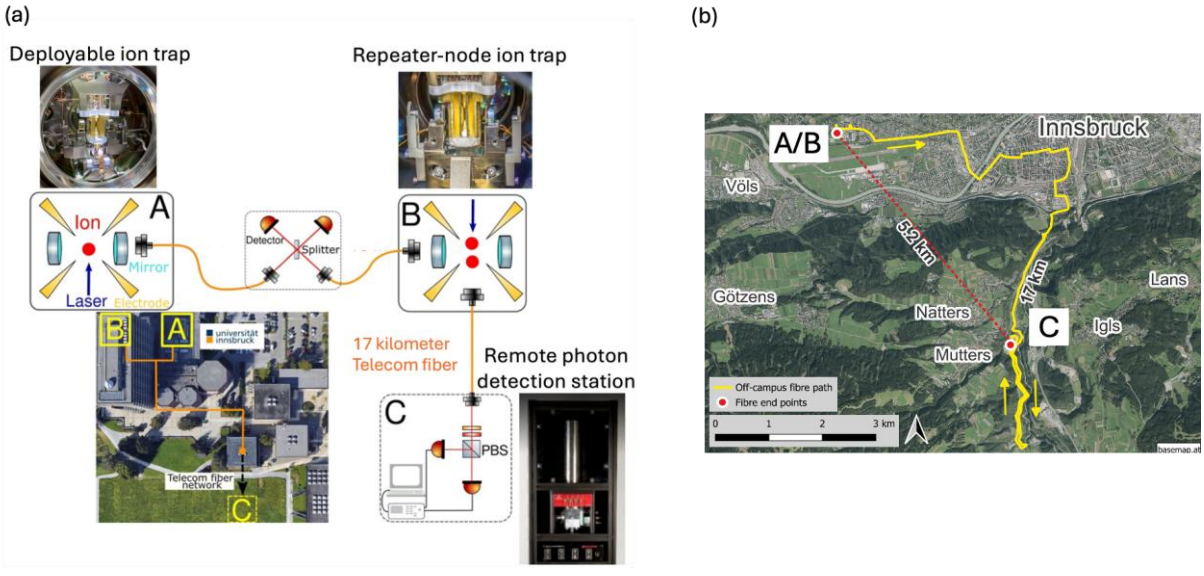

Figure 1. ***The developed three-node network.*** *(a) Concept image. The two ion-trap systems (A and B) are located in the same laboratory on the University of Innsbruck (UIBK)'s Technik campus in the city of Innsbruck and are connected by a few tens of meters of optical fibers. The fibers bring photons from each system to shared photon detectors. Each ion trap contains an integrated optical cavity formed by two mirrors for photon collection and metal electrodes to trap the ions. The remote photon detection station (C) is located in an industrial estate outside Innsbruck and is connected by 17 km of commercially rented optical fiber. Small inserted map shows the relevant part of the UIBK Technik campus. (b) Map showing 17 km long optical fiber path (yellow line) between the UIBK's Technik campus (A/B) and the remote detection station (C) in a satellite village. The endpoints have a 5.2 km line-of-sight separation (dashed green line). Satellite images created with [OPG] using [QGIS].*

Development of the repeater-node ion trap, 17 km fiber link and remote photon detection station.

This section shortly presents key results that represent significant quantum repeater node developments, achieved using the central repeater ion trap (B), as well as development of the long-distance fiber network and remote photon detection station.

3.1. Repeater ion trap development

At the beginning of the QCI-CAT project, the repeater ion trap (B, Figure 1) had recently been moved into new labs at UIBK and had previously been used to demonstrate aspects of a telecom-wavelength quantum repeater using coiled optical fibers all within the same lab [Krut23a]. After setting up the system again in the new labs, we developed and demonstrated the following four significant new capabilities within the QCI-CAT project.

Development and demonstration of a technique for entanglement storage time extension. As described in [Krut23a], the time for which entanglement can be stored in qubits inside the repeater node ion trap (Figure 1, B) is a critical parameter to enable long-distance networks. We developed and implemented a method to radically extend that storage time using a radio-frequency drive to dynamically decouple qubits defined in the electronic-spin ground-state manifold of $^{40}Ca^{+}$ ions in our prototype. The technical details underlying this work are presented in Johannes Helgert's master's thesis [Helg24], and we are currently writing up a research paper [Bate26] showing storage of ion-photon entanglement for 5 seconds (two orders of magnitude longer than previously achieved in a cavity-integrated ion trap).

Demonstration of multimode quantum networking over 101 km. The time for information to travel between the distant nodes of quantum networks presents a significant limit to the rate at which entanglement, and thus unconditionally secure keys, can be established across them. In our project paper [Krut24a] we demonstrated a technique to overcome this limit by distributing multiple photons, each entangled with a different co-trapped ion, in our repeater node ion trap, thereby achieving a record 101 km distribution of ion-photon entanglement. A short article about this work for the general public can be found here: https://physics.aps.org/articles/v17/s44

A photon-interfaced multi-qubit register. The ability to increase the number of qubits inside a quantum repeater node from the previous state of the art of two is a key step. In our project paper [Cant25a] we demonstrated a method to connect the quantum states of a register of trapped-ion qubits (in our repeater node prototype) to travelling photons; this method is scalable in qubit number. A short article about this work for the general public can be found here: https://physicsworld.com/a/ten-ion-system-brings-us-a-step-closer-to-large-scale-qubit-registers/

Generation of multipartite entanglement from a trapped-ion node. In this project paper preprint [Cant26] (currently under peer-review) we show that our trapped-ion systems are not only capable of distributing bipartite entanglement in future quantum repeater chains but also can function as a factory node and distribute *multipartite entanglement* to remote nodes. Specifically, we program the system to generate genuinely multipartite entangled Greenberger-Horne-Zeilinger (GHZ) states of three path-switchable photons and verify them using custom-designed entanglement witnesses. These photons can, in the future, be used to establish stored multipartite entanglement between remote matter-based nodes. Our results pave the way for the use of ion-trap systems to enable multipartite entanglement distribution in future quantum local area networks.

3.2. Deployed fibers and remote detection station development

There are two co-propagating 17-km long fiber channels (Figure 1, yellow line). One is used to transport single photons to the remote photon detection station; the other is used to return classical (laser) signals in the other direction. Both fiber channels are SMF28 single mode, suitable for the transmission of the central telecom C-band wavelength of 1550 nm. At each end there are 'last mile' fibers that we had installed across the UIBK campus and through the building housing the remote detection station, each a few hundred meters long. With the exception of these 'last mile' fibers, the fiber channels are rented from the local municipal services company (2 k€ per month), are part of the pre-existing fiber infrastructure in Innsbruck and are dark in the sense that they are used for our purposes exclusively. Details on our characterisation of the relevant properties of the fibers (transmission efficiency, light pollution and polarisation stability) are provided in Tatjana Runggaldier's master's thesis [Rungg25] and in our paper draft [Kodok26], which is provided in draft form in Appendix B. In summary, the total photon transmission efficiency at 1550 nm is 0.192(3), the total unwanted background counts introduced by the fiber through a final 1.5 GHz filter are below one per second, and the polarisation dynamics are remarkably stable over timescales of tens of minutes. Specifically, over four days of measurement, the fidelities between the transmitted polarisation states measured ten minutes apart were greater than 0.999 in 96.1% of the cases. For more details see [Kodok26], a current draft of which is given in Appendix B of this document. Our scheme for periodically stabilising the polarisation of light transmitted through the deployed fibers [Rungg25] was developed with support from project partner Qtlabs.

The remote photon detection station consists of two 19-inch racks, each approximately 2 m tall. One rack contains photon polarisation analysis optics. The other rack contains an array of superconducting nanowire single photon detectors. The entire setup is controlled remotely and housed inside an office with a wall-mounted air conditioning unit. More details on the remote photon detection station are provided in [Rungg25].

4. Demonstration of a distributed quantum-repeater node

While the new deployable ion-trap node was being developed, we replaced its role in the three-node network (A-B-C) with a second photon detection station that lies within the same lab and performed a repeater node demonstration over the deployed QCI-CAT network. Specifically, Node A was replaced with a photon detection station. The repeater node demonstration consisted of two distinct steps. First, the **repeater ion trap** (B) established entanglement with its neighbouring nodes (A and C) separately: independent photons were delivered to each photon detection station, and each of those photons was entangled with a different co-trapped ion in the repeater ion trap. Second, we performed entanglement swapping at the repeater ion trap, thereby establishing entanglement directly between the remote photons detected at A and C. The entanglement-swapping operation corresponded to a deterministic Bell-state measurement performed on the two co-trapped ion qubits, involving a laser-driven quantum-logic gate operation that entangled the ions, followed by logic-state readout via fluorescence detection of the ions' state. The results verified entanglement between the photon detected off-campus at node C and the photon detected in the lab. To the best of our knowledge, this is the first time that a trapped-ion repeater node has demonstrated its capabilities involving photons sent outside of a lab environment and constitutes a clear demonstration of repeater capability across the QCI-CAT network.

These results are currently being written up for submission to a peer-reviewed scientific journal [Kodok26]. The current draft of the paper [Kodok26] is included in Appendix B of this document. Specifically, the main text of the paper draft is presented in its original format. The abstract, conclusion and ten-page appendix are not shown, as they are currently being finalised.

The main results in the paper draft are:

- Relevant characterisation of the deployed fiber network, including light transmission efficiency, light pollution at the single photon level, and polarisation dynamics of transmitted light.
- Establishment and characterisation of entanglement between a single trapped ion and a single 1550 nm photon distributed over the deployed fiber network.
- Establishment and characterisation of entanglement between two separate single photons, one of which is distributed over the fiber network, using a trapped-ion quantum repeater node.

5. Development of a deployable ion-trap repeater node

All previous demonstrations of trapped-ion repeater nodes (ours [Krut23a] and another [Berg24]) have employed ion traps that are not suitable for direct transfer outside of the laboratory environment: e.g., employing bulky lasers, optics, and vacuum chambers on optical tables in a precisely stabilized environment. To enable near-term deployment of ion-trap repeater nodes outside of the laboratory, it is key to develop compact and robust prototypes that can in the future be deployed in a data-centre environment.

We developed and demonstrated a rack-mounted cavity-integrated trapped-ion node, yielding a compact setup that removes the need for optical tables. This deployable ion trap serves as Node A of our QCI-CAT network. The design, construction and operation of the rack-mounted cavity-integrated ion-trap network node was achieved in a collaboration between us (UIBK) and the local spin-off company Alpine Quantum Technologies (AQT). The design and construction of this node was supported by the EU Quantum Flagship project Quantum Internet Alliance[1], while the QCI-CAT funding supports its implementation within a repeater-node demonstration. The design constitutes an improved and considerably more compact version of the existing Node B ion-trap repeater node: it features a near-concentric cavity and linear ion trap mounted on a single vacuum flange, with a focus on precision alignment and vibrational rigidity.

The process of bringing up the system to operation included the following key steps:

- Construction of the trap and the cavity.
- Assembly of the rack-mountable cavity-coupled ion trap system under vacuum, involving a high-temperature bake which the cavity survived without measurable misalignment (no drop in its finesse).
- The trapping of ions and verifying the repeatability of the process and sufficient ion lifetimes.
- Stabilising the cavity length in the rack environment, verifying that the cavity can be locked to a fraction of its natural 854-nm linewidth of 70 kHz.
- Rack-mounting all available equipment.
- Setting up the control hardware and software.

The final system comprises two 19-inch racks: one rack for lasers, optics and most of the experiment control hardware; and one rack for the ion-trap module and related RF and DC electronic sources. An image of the final system is presented in Figure 2 below, showing the core parts of the system.

[1] Currently co-funded by the European Union's Horizon Europe research and innovation programme under grant number 101102140.

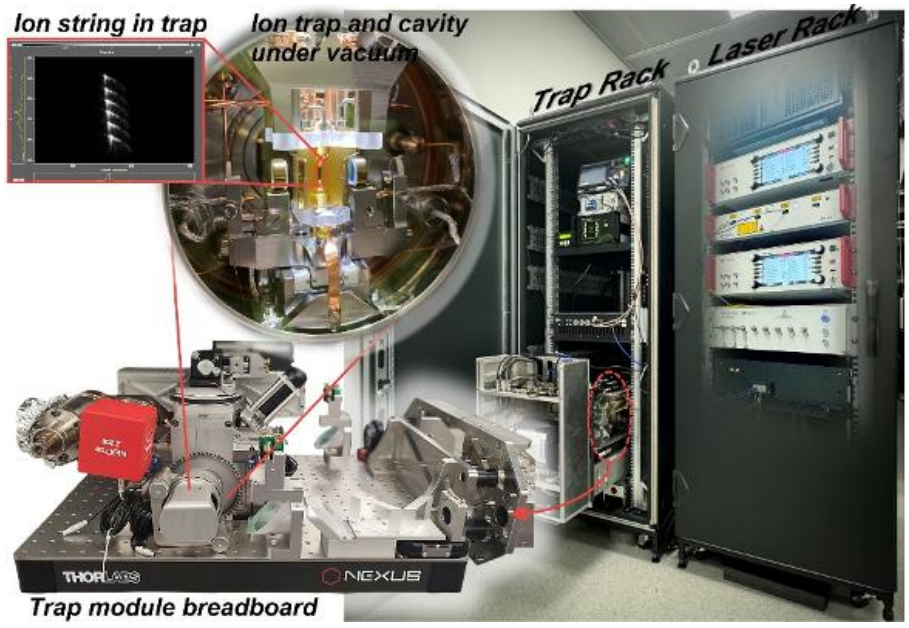

Figure 2. ***The developed deployable ion-trap repeater node****. The trap rack contains the ion-trap modules and related electronic sources to drive the ion trap and cavity. The laser rack contains lasers, laser optics and most of the experimental hardware. The inset ion string image shows 6 individual $^{40}Ca^{+}$ ions fluorescing in the trap, arranged in a linear string with inter-ion spacings of a few micrometers.*Key results achieved with the deployable system include:

- Ion-photon entanglement, the building-block operation for our repeater-node prototype, was generated and characterised following the protocol previously pioneered at UIBK [Stute12]. The polarisation of a single 854 nm photon (corresponding to the wavelength of the $^{40}Ca^{+}$ $4^2P_{3/2}$—$3^2D_{5/2}$ transition) is entangled with the internal electronic qubit state of a trapped ion. A fidelity of 98.2(2)% was measured with respect to the ideal maximally entangled state, far above the classical threshold of 0.5.
- Photons emitted by the system have successfully been converted to the 1550 nm telecom c-band wavelength. The underlying polarisation-preserving single-photon frequency-conversion technique employed is described in [Krut24a]. However, for this recent demonstration, the stabilised pump laser system described in the next section was employed as well as a newly developed, compact and more efficient photon conversion setup.

6. Towards linking the two ion traps

Our teams are currently working full time in the lab to establish the last connection in our QCI-CAT network: between the ion-trap repeater node (B) and the new deployable ion trap (A). Success will correspond to the establishment of entanglement between an ion in the repeater ion trap and an ion in the deployable trap. This entanglement will be established via the emission of an ion-entangled photon from each trap, followed by the injection of both photons into a beamsplitter and subsequent detection of the two photons in the beamsplitter output ports. Such a two-photon detection heralds the establishment of remote ion-ion entanglement, via entanglement swapping. While we have previously demonstrated this technique, using a different ion trap system and photons only at their natural 854 nm wavelength [Krut23b], now we take two significant steps forward. First, one ion trap is a compact deployable system. Second, the photons will both be converted to 1550 nm, and they will travel over a total of 50 km of coiled optical fiber before detection. This demonstration thus represents entanglement of trapped-ion repeater nodes over a metropolitan-scale fiber length.

A schematic of the experimental setup that is currently being used in the lab is shown below in Figure 3. **Key results so far include:**

1. **Design, construction and testing of a frequency-stable 1901 nm pump laser for distributed photon frequency conversion**. To enable entanglement to be established between repeater nodes, remote photon-frequency conversion must not introduce frequency noise into transmitted photons. We overcame this problem by producing 1901 nm light by difference frequency generation (DFG) using light from reference-cavity-stabilised 1550 nm and 854 nm lasers. The achieved 1901 nm linewidth is well below the 10 kHz target that we set. Crucially, that 1550 nm laser light can be easily distributed to remote repeater nodes in the future, enabling all nodes to produce their own stable 1901 nm pump laser light, by DFG with their own local 854 nm lasers.
2. **Synchronisation of the two ion-trap systems and delivery of time-controlled single photons:** new software was developed and tested in order to generate single photons from the deployable ion trap that are time synchronised with single photons from the repeater-node ion trap, as required for remote entanglement.
3. **Telecom-wavelength conversion using independent conversion setups.** Each ion-trap system has generated single photons, converted them to 1550 nm using independent conversion setups (each employing the stabilised pump), and detected those photons on the 'telecom Hong-Ou-Mandel (HOM) board' that lies at the centre of the final setup shown in Figure 3.

Current status and work in the final project weeks:

The complete experimental setup shown in Figure 3 is currently operational in the lab, and there is a detailed timeline of work for the establishment of remote ion-ion entanglement in the coming weeks. This timeline coordinates the work of 11 researchers on this setup. Currently, the individual parts of the setup are being optimised to improve their total transmission efficiency, and the single-photon detectors (SNSPDs) required for the entanglement demonstration are being transported from the remote photon detection station (C) to campus. First attempts to establish remote entanglement are planned to occur in the third and fourth week in March.

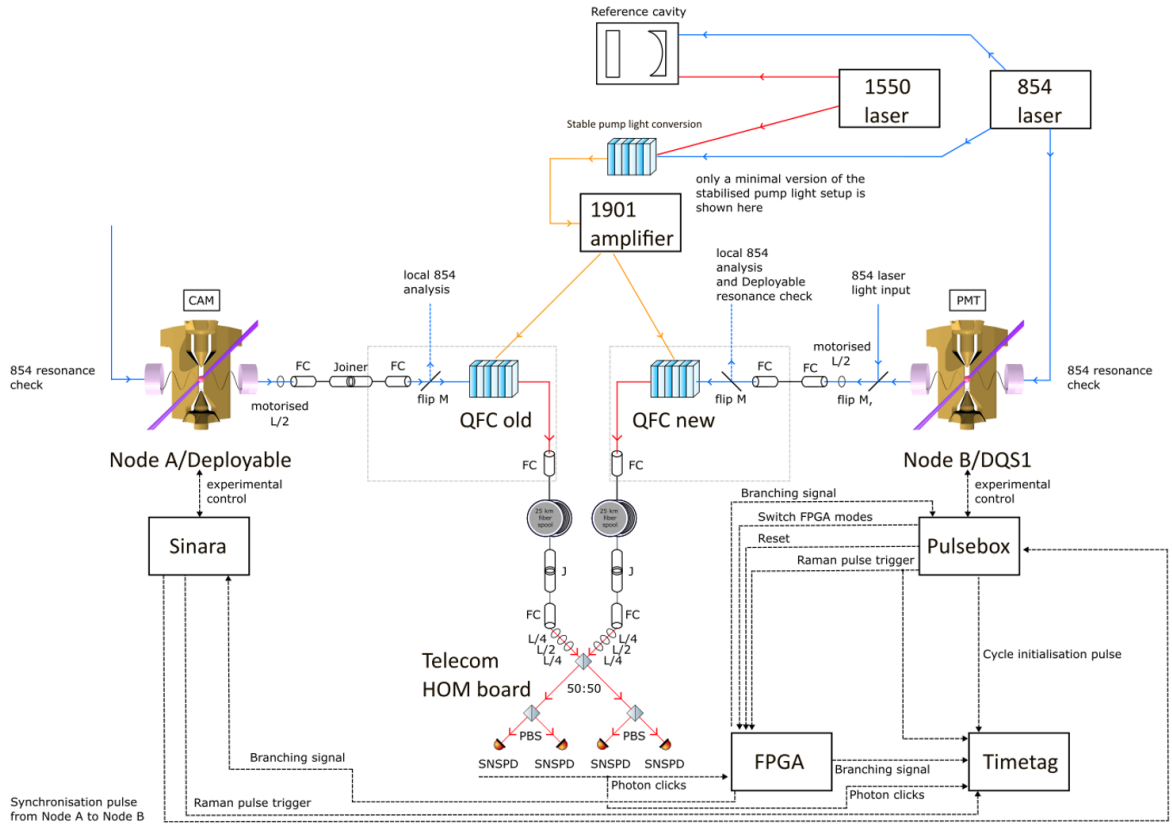

Figure 3. ***Schematic of the established experimental setup for entangling an ion in the deployable ion trap (A) with an ion in the repeater node ion trap (B, here labelled DQS1)****. A separate laser pulse at each ion ideally causes emission of an ion-entangled photon, which is subsequently converted to 1550nm (via QFC: quantum frequency conversion) exploiting an intrinsically stable 1901 nm pump laser. Photons traverse two 25 km long optical fiber spools (grey extended circles), are injected into a 50:50 beamsplitter (on Telecom HOM board), and are detected by one of four superconducting nanowire single photon detectors (SNSPDs), heralding remote ion-ion entanglement. Sinara and Pulsebox are central computer control systems for each ion trap. Photon detection events are recorded on a time tagger, and a field programmable gate array (FPGA) triggers ion-qubit readout conditional on specified combinations of photon detection events.*

Summary

We developed one prototype trapped-ion quantum repeater node ('deployable ion trap') and significantly extended a second prototype node ('repeater ion trap'). Specifically, in the first case, we designed, built, and demonstrated a compact rack-mounted node prototype suitable for future deployment out of the lab. In the second case, using the established repeater-ion-trap prototype, we developed and demonstrated four new techniques that significantly advance the state of the art in repeater technology. These results are captured in the publications [Krut24a, Cant25b, Cant25b, Bate26], and master's theses [Helg24, Rung25]. Separately, we built a distributed fiber network across the city of Innsbruck and used it to demonstrate the correct functioning of a trapped-ion repeater node. This is the first demonstration of such a repeater node involving optical fibers distributed outside of a laboratory environment. Finally, we are currently running experiments to establish entanglement between the two prototype nodes, over a 50 km long telecom-wavelength fiber spool. These results show that trapped-ion repeater technology is ready to move outside of the lab and sufficiently mature for direct integration with existing fiber networks.

Appendix A - List of Acronyms

Table 1 List of Acronyms

Acronym	Meaning
DFG	Difference Frequency Generation
QFC	Quantum Frequency Conversion
QKD	Quantum Key Distribution
UIBK	University of Innsbruck

Appendix B – Paper draft

Trapped-ion based quantum repeater node across a 17 km-long metropolitan fiber

F. Kodokkat,[1] T. Runggaldier,[1] A. Winkler,[1] F. Bernecker,[1] J. Bate,[1] M. Canteri,[1] J. Helgert,[1,2] T. E. Northup,[1] V. Krutyanskiy,[1] and B. P. Lanyon[1,*]

[1] *Institut für Experimentalphysik, Universität Innsbruck, Technikerstr. 25, 6020 Innsbruck, Austria*
[2] *LaserLaB, Department of Physics and Astronomy, Vrije Universiteit Amsterdam, De Boelelaan 1100, 1081 HZ Amsterdam, Netherlands*

(Dated: March 11, 2026)

The abstract has not yet been written.

Significant efforts are underway to develop light-matter quantum networks, consisting of distributed nodes—each housing matter-based quantum registers for storing and processing quantum information—interconnected by photonic links [1, 2]. Networks of this type, operating over distances ranging from a single city to continental scales, would enable powerful applications in secure communication [3], distributed computing [4], precision sensing [5], and timekeeping [6]. Prototype city-scale light-matter networks are already under development [7–11]. A central strategy for extending the reach of these emerging networks is the implementation of quantum repeaters [12]: devices that enable long-distance quantum communication by establishing entanglement over short segments and stitching them together, thereby circumventing the impossibility of copying or amplifying unknown quantum states. Demonstrations of several key elements of quantum-repeater architectures have been realized in laboratory-based experiments [13–16].

Registers of electrically trapped atomic-ions are a powerful candidate platform for realising quantum network nodes. They can each function as prototype quantum computers [17] and interface their quantum states with optical-wavelength photons [18, 19], enabling entanglement of ions in remote vacuum chambers [20–24] and supporting state-of-the-art quantum networking applications [25–28]. Moreover, the ability to interconnect the quantum states of trapped-ion qubits with telecom-wavelength photons that suffer minimal loss in standard optical fibers [29, 30] enables the establishment of ion-photon entanglement [30, 31] and ion-ion entanglement [28] over tens of kilometers of coiled optical fiber. Trapped ions could also serve as advanced quantum repeaters [32]. Indeed, elementary trapped-ion repeater nodes have been recently demonstrated [16, 33]. The repeater node sits in the middle of a two fiber segments and establishes entanglement between photons distributed to each end, via the repeater technique. Such nodes could in future be chained to establish ion-ion entanglement over longer distances [16].

In this work, we demonstrate the trapped-ion quantum repeater node of [16] with one of its fiber segments deployed across and outside of a city. Specifically, the repeater node establishes entanglement between a photon detected after over a 17 km deployed fiber and a second photon detected in the lab containing the repeater node, via the repeater technique. In future, the photons could be sent out of the lab in different directions, to connect e.g., distributed ion nodes across or outside the city. The rest of this paper is structured as follows. First, the experimental setup of the network described. Second, the deployed fiber is characterised in terms of its transmission efficiency, polarisation dynamics and intro-

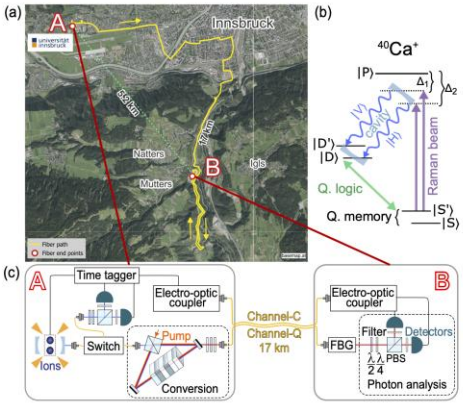

FIG. 1. **The two node quantum network**. (a) Satellite image created with [34] using [35]. Nodes A and B are located in separate buildings, connected via 17 km-long optical fibers (yellow line) and have a 5.2 km-line of sight separation (dashed green line). (b) $^{40}Ca^+$ energy-level diagram showing photon generation process via a cavity-mediated Raman transition: $|S\rangle = |4^2S_{1/2,m_j=-1/2}\rangle$, $|S'\rangle = |4^2S_{1/2,m_j=+1/2}\rangle$, $|P\rangle = |4^2P_{3/2,m_j=-3/2}\rangle$, $|D\rangle = |3^2D_{5/2,m_j=-5/2}\rangle$, $|D'\rangle = |3^2D_{5/2,m_j=-3/2}\rangle$. (c) The setup at location A consists of a linear Paul ion trap (four yellow electrodes), with an integrated optical cavity comprised of two mirrors. Collected photons are switched either to a polarisation analysis setup—containing polarising beam splitter (PBS), half- and quaterwave plates ($\frac{\lambda}{2}$ and $\frac{\lambda}{4}$) and fiber-coupled photon detectors—or to a telecom wavelength conversion setup (854 nm to 1550 nm). The setup at location B consists of a fiber bragg grating (FBG, 1.5 GHz bandwidth) followed by a second polarisation analysis setup. 12 nm bandpass filters are situation before each detector.

* Correspondence should be sent to ben.lanyon@uibk.ac.at

duced light pollution. Third, the quality, efficiency and rate with which ion-photon entanglement is distributed across the deployed fiber is investigated. Fourth, the repeater node results are presented. Finally, there is a short discussion and outlook.

Elements of trapped-ion quantum networks have recently been demonstrated in a deployed scenario; using optical fibers distributed outside of laboratories and thus exposed to uncontrolled environmental conditions. Using the trapped ion system in the present work, two $^{40}Ca^{+}$ ions in separate buildings 230 m apart were entangled via the transmission of 854 nm photons through a deployed optical fiber [23]. Separately, entanglement was established between a single $^{40}Ca^{+}$ ion and a 1550 nm photon distributed across a 14-km-long urban fiber link across Saabrücken, Germany [10]. Finally, in Durham, USA, entanglement was established between a $^{88}Sr^{+}$ ion and a 1092 nm photon distributed across a 2.8 km long urban fiber link [36]. The present paper demonstrates the action of a trapped-ion quantum repeater node across an urban fiber link distributed across Innsbruck, using 1550 nm photons and two co-trapped, and individually-addressed $^{40}Ca^{+}$ ions.

I. EXPERIMENTAL SETUP

A detailed description of the experimental setup is presented in Appendix Section A.I and now summarised. Our deployed network consists of a 17km-long optical fiber path that connects a laboratory in the city of Innsbruck (location A) to an office located in a satellite village outside the city (location B), as shown an Figure 1(a). There are two co-propagating 17-km long fibers. One is used to transport single photons from location A to B, and is henceforth referred to as Channel Q. The other is used to return classical (laser) signals in the other direction, henceforth refereed to as Channel C. Both fibers are SMF28 single mode, suitable for the transmission of the central telecom C-band wavelength of 1550 nm. The fibers are rented from the local municipal services company, are part of the preexisting fiber infrastructure in Innsbruck and are dark in the sense that they are used for our purposes exclusively.

Location A. The lab setup at location A includes a linear Paul ion trap with an integrated 20mm-long optical cavity for the collection of ion-emitted single photons at 854 nm [37]. Up to two $^{40}Ca^{+}$ atoms are co-trapped in this work, each positioned at the maxima of a vacuum-cavity standing wave of the optical cavity at 854 nm. A photon can be generated from either one of the atoms via a bichromatic cavity-mediated Raman transition (Fig. 1(b)) [38]. Here, a micron-focused Raman laser pulse applied to a chosen ion ideally generates the maximally entangled ion–photon state $|\psi_k(\phi)\rangle = 1/\sqrt{2}\left(|\mathrm{DV}\rangle + e^{-i\phi}|\mathrm{D'H}\rangle\right)$, where $|\mathrm{D}\rangle$ and $|\mathrm{D'}\rangle$ are the respective metastable Zeeman states $|3^2\mathrm{D}_{5/2}, m_j = -5/2\rangle$ and $|3^2\mathrm{D}_{5/2}, m_j = -3/2\rangle$, $|\mathrm{V}\rangle$ and $|\mathrm{H}\rangle$ are the vertical and horizontal polarization components of a photon emitted into the cavity vacuum mode, and ϕ is a tunable phase [38]. After the photon exits the cavity through the output mirror, it is coupled into a single-mode fiber-coupled optical switch and sent either to a polarisation-analysis setup or a photon frequency conversion setup, which are described later. An acoustooptic deflect allows the focal point of the Raman laser to be switched to the co-trapped ion in a few microseconds, allowing for generation of a second ion-entangled photon.

A broadly-focused laser beam at 729 nm, which ideally couples equally to both ions, is used both to transfer the ion-qubit between different encodings and to perform quantum logic operations, as now described. For ion-qubit storage on the millisecond timescale, the metastable qubit ($|D\rangle/|D'\rangle$) is transfered down to the ground state qubit ($|S\rangle/|S'\rangle$, Figure 1(b)), which serves as a quantum memory. Dynamical decoupling extends the coherence time of the ground state qubit, realised with radio frequency (RF) pulses at 11.6 MHz generated by a current-carrying coil that lies outside the vacuum chamber. Entangling quantum logic gates are realised on optical qubits, encoded in superpositions of $|S\rangle$ and $|D\rangle$. Specifically, A 205 mus-long 729 nm laser pulse realises a two-qubit entangling Mølmer–Sørensen gate [39] via off-resonant driving of the outermost radial COM mode of the ion string. Ion-qubit readout is performed on optical qubits and consists of optional 729 nm single-qubit rotations to set the desired measurement basis, followed by state detection via electron shelving. During electron shelving, the $|S\rangle$ state fluoresces 393 nm photons while the $|D\rangle$ state does not. The fluorescence state of each ion (bright or dark) is determined individually, via imaging onto a digital camera, taking 2.5 ms.

The polarisation analysis setup at location A consists of free-space waveplates, a polarising beam splitter and two fiber-coupled nanowire single photon detectors optimised for 854 nm. The photon frequency conversion setup converts incoming fiber-coupled 854 nm photons to outgoing fiber-coupled 1550 nm photons, in a polarisation-preserving fashion. The conversion process is realised via difference frequency generation involving a 1901 nm pump laser and a periodically-poled LiNb crystal in Sagnac configuration. More details can be found in the Appendix A.I.1. The converted telecom-wavelength photons are then injected into Channel Q with a fiber joiner.

Location B. The setup at location B includes a similar photon polarisation-analysis setup, to the one in the lab, but now optimised for 1550 nm wavelength photons. At the input of that setup there is an optical bandpass filter (Fibre Bragg Grating) centred at 1550 nm, with a bandwidth of 1.5 GHz. Detector clicks are converted to optical signals via an electro-optic coupler and sent back to location A via Channel C. The received signals at location A are recorded on a timetagger and used to trigger readout of the ion-qubit states. The travel time for single photons, or return optical signals, to traverse the fiber path

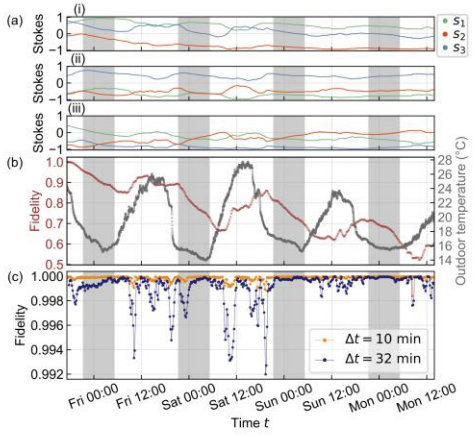

FIG. 2. **Polarisation dynamics of laser light through the 17km-long fiber.** Grey shaded regions show nights. (a) Output Stokes parameters, for input polarisations (i) horizontal, (ii) diagonal and (iii) right-circular. (b) Red line and left axis shows the fidelity between the polarisation process implemented by the Channel C at time t and the first process measured ($F(E_t, E_{t_0})$). Grey data points show the outdoor temperature measured in downtown Innsbruck [40]. (c) Process fidelity between data taken ten minutes apart (blue data) and 32 minutes apart (yellow data). Specifically, $F(E_t, E_{t-\Delta t})$ for Δt = 10 min and 32 min.

between Locations A and B is 82 µs. That travel time is calculated using a refractive index of 1.468 at 1550 nm for the 16.74 km-long SMF 28 fiber of Channel Q.

Polarisation stabilisation setup. Section II.A provides additional details on our setup for characterizing and stabilizing the polarization dynamics in Channel Q, which is not shown in Figure 1b). In summary, a flip mirror at the input of Channel Q allows polarized 1550 nm laser light to be injected at Location A, while a second flip mirror at the output directs the light to a polarimeter at Location B. Any desired input polarization state can be prepared using waveplates, and both the waveplates and flip mirrors are remotely controlled.

II. RESULTS

The results section contains three subsections. The first subsection presents our characterisation of the relevant properties of the deployed optical fibers. The second subsection presents the establishment of entanglement between a single trapped ion a location A and a telecom-wavelength photon detected at location B. The third subsection presents our demonstration of a repeater node, in which two co-trapped ions are used to establish entanglement between a photon detected at location B and a separate photon detected at location A.

II.A. Channel characterisation

This subsection presents the results of experiments that characterise key properties of the deployed fibers, before sending single photons through them. Specifically, the transmission efficiency and polarisation dynamics of laser light sent through the fibers is presented, followed by the amount of background light in-coupled and transmitted through them, at the single photon level.

Transmission efficiency. The transmission efficiency of Channel Q is determined by injecting 1550 nm laser light into its input in the lab and measuring the power directly at the output at location B, as detailed in Appendix A.I.4. The result is a ratio of output to input power of P_6 = 0.192(3), which we take as the transmission efficiency for Channel Q for all subsequent calculations. A separate series of measurements of individual sections of Channel Q (A.I.4), using optical time domain reflectometry (OTDR), yielded a higher transmission efficiency of 0.239. The OTDR-derived value does not include additional losses due to connecting the individual sections together.

Typical attenuation rates for 1550 nm light traversing SMF28 fiber is 0.2 dB/km, which would yield an ideal transmission efficiency over the 16.74km length of Channel Q of 0.463. The lower measured efficiency (P_6) is attributed to losses in the splices and connectors along the channel. Typical attenuation rates for the ion-emitted wavelength of 854 nm in wavelength-optimised standard silicon fiber is 3 dB/km, which would yield an ideal transmission efficiency over the 16.74km length of 1×10^{-5}. Photon conversion to the 1550 nm is therefore critical.

Polarisation stability. Since we encode qubits into the polarisation of transmitted photons, any polarisation rotations imparted by the channel should be stable over the timescale of measurement runs. Instabilities in polarisation rotations in optical fibers can be caused by dynamically evolving stresses and strains modifying the fiber's birefringence. We study the dynamical evolution of the polarisation of laser light transmitted through the deployed fibers, over a period of several days. During this time, we repeatedly perform tomography of the process [41] implemented by the fiber channel on the polarisation of transmitted 1550 nm laser light, as now summarised and detailed in Appendix A.I.3.

Each process tomography run involves injecting a set of six different polarisations of 1550 nm laser light into one of the deployed fibers (channels) and, in each case, measuring the output Stokes parameters using a polarimeter. The corresponding Choi process matrix E [41] is obtained via the maximum likelihood technique. Obtaining each process matrix E takes 28 seconds, limited

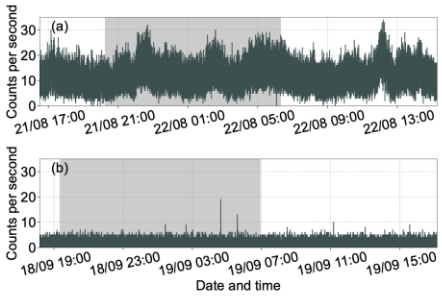

FIG. 3. **Background photons introduced by the Channel Q.** a) Total detector counts recorded at node B a) without the Fiber Bragg grating filter (FBG) in place and b) with the FBG in place. Without the FGB, the filtering bandwidth is set by the 12 nm filters. With the FBG, the filtering bandwidth is 14(2) pm (b). Night time is shaded in grey. The sum of both detector in the polarisation analysis setup is shown.

almost entirely by the time for waveplate rotation used to prepare the different input states. We quantify the similarity of two process matrices measured at different times, E_1 and E_2, via the process fidelity $F(E_1, E_2) = \left(\mathrm{tr}\sqrt{\sqrt{E_1}\,E_2\,\sqrt{E_1}}\right)^2$ [41].

Process tomography runs were performed over a period of four days through Channel C. The start times of the runs are spaced by ten minutes. The recorded Stokes parameters for three example input polarisations are presented in Figure 2(a). All reconstructed process matrices are well described by unitary rotations. Specifically, the fidelity F between each process matrix and an arbitrary single qubit unitary U lies between 0.9945 and 0.9980. We now consider the *initial process fidelity* $F(E(t), E(t_0))$, where $E(t)$ is the process matrix recorded at time t and $E(t_0)$ is the the first one measured. Figure 2b compares the dynamics of this initial process fidelity with the outdoor air temperature measured near location A. The initial process fidelity is seen to display oscillatory behaviour with a period of approximately one day. This behaviour is partially correlated with the temperature: both values rise and fall on approximately the same timescales and, over some intervals, exhibit similar dynamics. There is a temporal delay between variations in the temperature and those in the fidelity, and the fidelity does not always have the same features as the temperature.

To better see the dynamics over shorter timescales, we next consider the fidelity between processes taken a time Δt apart: $F(E(t), E(t - \Delta t))$. When considering processes ten minutes apart ($\Delta t = 10$, Figure 2c orange lines) the fidelity remains greater than 0.999 in 96.1% of the cases over four days. The polarisation rotations imparted by the deployed fiber are thus remarkably stable on this timescale, with only rare cases resulting in infidelities greater than 0.001. Even for processes 30 minutes apart ($\Delta t = 30$, Figure 2c blue lines) a fidelity of greater than 0.99 is achieved in 97.8% of the cases. The results presented here are for Channel C, while single photon qubits are later sent through Channel Q. However, we find that the polarisation stability metrics are essentially equivalent for Channel Q, which copropagates with Channel C along its entire path to the best of our knowledge.

Polarisation rotations imparted by optical fibre can be stabilised by first characterising them and then correcting them via feedback to controlled birefringent elements, as demonstrated in e.g., [10, 42–45]). Given the stability of our deployed fibers, we perform polarisation stabilisation runs at intervals of tens of minutes or more. Each run involves two steps. In the first, we characterise the process, $E(t)$, implemented by the channel on the polarisation of injected 1550 nm laser light at time t, as previously summarized. We then numerically calculate the nearest unitary rotation U_t to $E(t)$. In the second step, we correct by setting the waveplates immediately before the input of Channel Q (Figure 1c) to implement the inverse U_t^{-1}, such that the combination of waveplates and channel ideally realise the operator $U^{-1}U_t = \mathbb{1}$, where $\mathbb{1}$ is the one-qubit identity operator. The characterisation step takes 28 seconds, the correction step takes 8 seconds, yielding a total time for each stabilisation run of 36 seconds. This time is entirely dominated by waveplate rotation time and could be significantly sped up if desired (e.g., see [10]). In between stabilisation runs, experiments involving single photon transmission can take place.

Background light. Light can couple into an optical fiber from sources along its path, such as room lights and data traffic in co-propagating fibers. This light pollution can lead to photons exiting the fiber that lie within the final filtering bandwidth, acting as a background to the signal photons emitted by the ion. We measure this background using the setup in Figure 1c, by blocking the input of Channel Q in the lab and recording the photon detector clicks of both detectors at location B.

In the first measurement run, the background counts were recorded over a day without the fiber Bragg grating (FBG) filter at the output of Channel Q. The filtering bandwidth in this case is set by the remaining 12 nm bandpass filters centred at 1550 nm. The recorded counts, shown in Figure 3(a), have an average value of 10.80(1) cps. In the second measurement run, the FBG filter is included which has a bandwidth of 14(2) pm at 1550 nm (1.5 GHz). The recorded counts, shown in Figure 3(b), are reduced to an average of 1.208(4) cps which is consistent with the sum of intrinsic detector dark counts, of 1-2 cps. Therefore, within a 1.5 GHz filtering bandwidth, we do not detect any background photons introduced by Channel Q. That filtering bandwidth is orders of magnitude broader than the bandwidth of photons emitted by our cavity-integrated ion trap (0.1MHz) and thus ideally causes no loses due to spectral filtering.

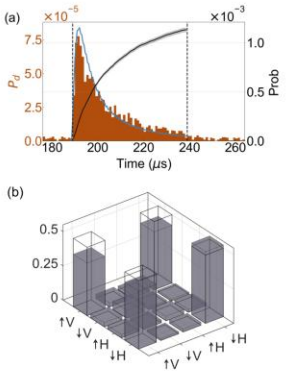

FIG. 4. **Observation of ion-photon entanglement across the two node network**. (a) Histrogram of single photon detection events at node B. Probability density is shown on the left vertical axis: the number of counts normalized by the number of attempts and by the time-bin width of 1 µs. Red bars show data. Solid blue line shows a theoretical model and the solid black line (right vertical axis) represents cumulative photon detection probability with error bars as grey shading. DBSM is performed within the window indicated by the dashed black lines. (b) Absolute value of density matrix of the reconstructed joint two-qubit ion-photon state. The wire mesh shows the ideal Bell state.

II.B. Distributed ion-photon entanglement

Experimental details. Now we report on the establishment of entanglement between a single photon delivered to location B and a single trapped ion at location A. A single ion is loaded into the trap. The *experimental sequence* begins with state initialisation by Doppler cooling and optically pumping the ion, taking 3.24 ms. The sequence continues with a loop in which up to 10 attempts are made to establish remote ion-photon entanglement. In each iteration of the loop optical pumping (30 µs) and repumping pulses (60 µs) are performed followed by a Raman laser pulse of length 50 µs which ideally generates the ion-photon entangled state $|\psi_k(\phi)\rangle$. The photon is ideally converted to 1550 nm, sent into channel Q and detected at location B after a travel time of 82 µs. That travel time is calculated using a refractive index of 1.468 at 1550 nm for the 16.74 km-long SMF 28 fiber of Channel Q. In the case in which either of the two photon detectors at location B fire within the expected 50 µs arrival time window, a signal is sent back to location A via Channel C (82 µs travel time), the sequence exits the loop, and the ion qubit is measured. Ion-qubit measurement begins by first mapping the metastable qubit to the optical qubit (5.2 µs), followed by an optional laser pulse to change measurement basis (3.1 µs) and finally state detection via electron shelving for 2.5 ms.

The remote ion-photon state is characterized via quantum state tomography, for which the experimental sequence is repeated for different measurement bases of ion and photon. The measurement basis for the detected photon polarisation qubit is set by the angles of the waveplates at location B. The measurement basis for the ion qubit is set by laser pulses. For state tomography, we measure in a total of 18 different ion-photon bases, corresponding to all combination of the three Pauli basis for the ion and the following six polarisation bases [H/V, V/H, +/-, -/+, R/L, L/R], where respectively +/− are diagonal and antidiagonal, and R/L are right- and left-circular polarisation. Swapped bases e.g., H/V and V/H, are measured by swapping the detector that receives the H or V photon via choice of waveplate setting, which allows for cancellation of any detector efficiency imbalances in the subsequent analysis. Tomographic reconstruction, via the maximum likelihood technique, yields the two-qubit ion-photon density matrix ρ^B_{i-ph}, where the B superscript clarifies that the photon is detected at location B.

We quantify the entanglement of the state via the concurrence C [46]. A concurrence above zero proves entanglement and a maximum value of one is achieved by the Bell states, or any state that is equivalent to a Bell state up to a tensor product of any single qubit rotations (e.g., $|\psi_k(\phi)\rangle$). The measured state ρ^B_{i-ph} is expected to deviate from the ideal state $|\psi_k(\phi)\rangle$ due to e.g., unitary rotations of the photon polarisation imparted by the fibers between the ion-trap's vacuum chamber and the input of Channel Q. To return the state to the familiar Bell-state form, we numerically search for the single qubit rotations which maximise the fidelity with the Bell state $|\psi_k(0)\rangle$. That is, we maximise $\langle\psi_k(0)|U\rho^B_{i-ph}U^\dagger|\psi_k(0)\rangle$, where $U = u_i \otimes u_p$ is a tensor product of single qubit rotations on the ion and photon, respectively. The obtained rotations are then used to rotate the measured state into the Bell form $\rho^{Bell}_{i-ph} = U\rho^B_{i-ph}U^\dagger$. These rotations do not change the entanglement content of the measured state, allow for the state to be easily visualised and for calculation of the fidelity. A fidelity $F = \langle\psi_0(\phi)|\rho^{Bell}_{i-ph}|\psi_k(0)\rangle > 0.5$, proves the existence of entanglement [47] and is equivalent to the fidelity that our state has with the nearest maximally entangled state. Statistical uncertainties in properties derived from the density matrix are estimated via Monte Carlo resampling [48], based on Poissonian photon counting statistics.

Polarisation stabilisation results. Tomographic measurements of the distributed ion-photon state were carried out, interleaved with four polarisation stabilisation runs: one at the beginning, one at the end and two in between. The results of the polarisation stabilisation runs show that the fidelity between two consecutively measured processes never dropped below 0.9999. There was therefore no significant change in the polarisation dynamics over the tomographic measurement run and this effect can be ignored.

Efficiency and rate. Over a total of 60 minutes, k = 2167496 attempts were made to deliver a photon to location B and N_d = 2454 detection events were recorded, corresponding to an average probability of $P_{ip} = 1.13(2)\times 10^{-3}$ for delivering an ion-entangled photon at an average rate of $0.6817\,\mathrm{s}^{-1}$. Out of those 60 minutes, 3.2 mins were used for periodic polarisation stabilisation, 12.05 minutes for other calibrations, 1.5 minutes for waveplate rotation to change photon-qubit measurement basis and 7.95 minutes to reprogram our central pulse generation control hardware. Thus only 35.3 minutes were spent running the photon distribution sequence, which yields an average photon delivery rate of $1.16\,\mathrm{s}^{-1}$. The temporal profile of the detected single photons at location B are shown in Figure 4(a). This single-photon wavepacket is presented as a probability density $P_d(t) = N_d/(\kappa \times \delta t)$, where N_d is the number of detection events registered in a time bin δt =10 µs and κ is the number of attempts to generate a photon. To obtain the simulated wavepacket in Figure 4(a), we numerically solve a model of the photon generation process, as detailed in Appendix A.II.3. In summary, the model is based on a master equation comprising 18 electronic states in the ion and two frequency-degenerate modes of the cavity [49]. All parameters in the model are independently measured via calibration experiments, except the photon detection path efficiency, such that there are no other free parameters within calibration uncertainties. The total probability of the simulate wavepacket shown in Figure 4(a) has been set such that it matches the measured value $P_{ip} = 1.13(2) \times 10^{-3}$.

Table 1 presents an efficiency budget for the expected maximum value of P_{ip}, where each row entry gives the efficiency of a distinct part of photon path, beginning the probability P_1 that the ion emits a photon into the cavity and ending with the average telecom photon detector efficiency (P_8). All of the values are obtained from independent calibration experiments (see Appendix A.II.4). The probability for generating a cavity photon is obtained from the same numerical simulation used to produce the simulated photon wavepacket in Figure 4(a). The product P_1 through P_8 yields the total expected maximum photon detection efficiency at location B of $1.8(2)\times 10^{-3}$. This is a maximal value, as the values P_i are obtained for isolated and optimised individual parts, and do not consider any additional losses incurred when connecting the parts together. We associate the lower measured value $P_{ip} = 1.13(2) \times 10^{-3}$ to these differences.

Density matrix, concurrence and fidelity. The absolute value of the tomographically-reconstructed ion-photon density matrix ρ_{ip}^{Bell} is presented in Figure 4(b). The state ρ_{ip}^{Bell} has a Bell state fidelity $F = 0.88(1)$ and a concurrence $C = 0.78(2)$, proving strong entanglement between the ion and remotely-delivered photon. To investigate the origins of state imperfections we performed calibration experiments and developed a model for the Bell state fidelity, as detailed in A.II.2 and now summarised. First, we tomographically-reconstruct the ion-photon state measured in location A before the photon converter. This state is then rotated to the Bell form state $\rho_{ip}^{B,Bell}$ in the same way as described above for the state ρ_{ip}^{B} but using newly numerically-obtained single-qubits rotations. For the state $\rho_{ip}^{B,Bell}$ we obtain a Bell state fidelity of 0.953(6), and 0.975(3) after subtracting background counts from the photon detectors in Location A. The background-subtracted state is our best estimate of the entangled state injected into the converter. Finally, we model the additional fidelity reduction due to the combination of that imperfect state, the additional photon loss on the path to Location B and the total detected photon detector background rate in location B (2.04(14) s^{-1}) extracted from the same data set used to produce Figure 4(b). The model predicts a remote Bell state fidelity of maximally $F = 0.905(8)$, which differs from the measured value of 0.88(1) by 0.025(0.013), which is not statistically significant. We conclude that the infidelity in the remote ion-photon entangled state ρ_{ip}^{Bell} is contributed by the photon background counts detected at Location B and imperfections in the state characterised at the output of the ion-cavity system. The infidelity due to background counts could be reduced in future by increasing the signal to noise ratio: either by using lower darkcount detectors or by reducing losses in the photon transmission. Identifying the causes of infidelities in the generated ion-photon state and developing a quantitative infidelity budget will require a separate study: we expect a range of different physical origins each contributing at the sub percent level, including imperfections of the laser-driven ion analysis pulses and photon polarisation analysis optics.

TABLE 1. Efficiency budget for the probability of generating an ion-entangled photon, transferring it over the deployed fiber and detecting it at the remote location B, for the experiment presented in Section II.B.

Part	Symbol	Efficiency
Cavity photon generation	P_1	0.59
To exit the cavity	P_2	0.43(3)
Path to QFC	P_3	0.61(3)
QFC	P_4	0.22(1)
Channel Q	P_5	0.192(3)
FBG	P_6	0.54(2)
Photon analysis board	P_7	0.62(2)
Average detector	P_8	0.82(2)
Total product	$\boldsymbol{P_{\mathrm{ip}}}$	**0.0018(2)**

II.C. Repeater node demonstration

We now report on our demonstration of a repeater node. Following the original proposal for a quantum repeater [50], the action of a central repeater node is to first establish bipartite entanglement between itself and its neighbouring nodes separately, exploiting its ability to store quantum information in memory, then perform en-

tanglement swapping to establish entanglement directly between its neighbours. Entanglement swapping is ideally realised via a deterministic Bell state measurement (DBSM) on the central repeater node's qubits.

In our network, following the approach of [16], the ion trap functions as a central repeater node and the two photon analysis stations play the roles of the neighbouring nodes. Entanglement is first established between one trapped ion and a photon delivered to the remote detection station (location B), as well as between a second, co-trapped ion and a photon detected in the local detection station (location A). A combination of laser-driven quantum logic gates and logical-state readout of the ion-qubits then realises the DBSM on the ion-qubits. There are four outcomes of the DBSM, each ideally yielding one of four orthogonal Bell states of the distributed photon qubits.

Setup. The employed experimental setup is the one shown in Figure 1(c), which differs from the setup used in the previous section in the following ways. Two ions are now loaded into the trap and the fiber-coupled optical switch is employed. The switch allows ion-entangled fiber-coupled 854 nm photons to be sent either to the local analysis board or to the photon conversion setup and subsequently into Channel Q. The switching time is on the order of a microsecond, allowing sequentially-emitted photons to take different paths. The switch has a transmission probability of 0.65(?). The transmission efficiency of the QFC setup for this experiment was significantly improved to 0.36(4), from the 0.22(1) value in the previous section, as described in A.I.1. The photon detection path efficiency budget for the repeater node experiment is thus the one in Table 1 with the addition of the switch transmisson factor, a modification of the QFC value to 0.36(4) and new simulated cavity photon generation efficiencies P_1^1 =XX and P_1^2 =XX for ions 1 and 2, respectively. Those new simulated values are discussed in Appendix A.III.4.

Repeater node protocol. The protocol is described in detail in subsection A.III.1 and is now summarized. The protocol has four parts: Initialisation, Loop 1, Loop 2 and DBSM. Initialisation prepares both ions in the electronic state $|S\rangle$ and the motional ground state of the radial centre-of-mass mode with highest frequency. Up to 20 attempts are then made in Loop 1 to deliver a 1550 nm photon to the remote detection station (location B). This first photon is ideally always emitted by and entangled with the same ion, referred to as ion 1. In the case of successful detection of that remote photon, up to 22 attempts are next made in Loop 2 to deliver an 854 nm photon to the local detection station (location A) that is entangled with the co-trapped ion (ion 2). During Loop 2, the qubit state encoded in ion 1 is stored in the ground state manifold and dynamical decoupling is executed to extend its coherence time. In the case of successful detection of the second photon at location A, both ion-qubits states are transferred into optical encodings and the DBSM is performed: First, the laser-driven two-qubit entangling Mølmer–Sørensen (MS) quantum logic gate [39, 51, 52] is applied; Second, the logical state of each ion qubit is measured via fluorescence state detection captured by the digital camera. Observing one of the four logical states of the ion qubits ideally heralds the projection of the polarisation of the remote photons into one of four orthogonal maximally-entangled states. The repeater protocol is now complete. Those photonic states are characterised via quantum state tomography, done by repeating the protocol for a range of polarisation analysis settings at the photonic nodes.

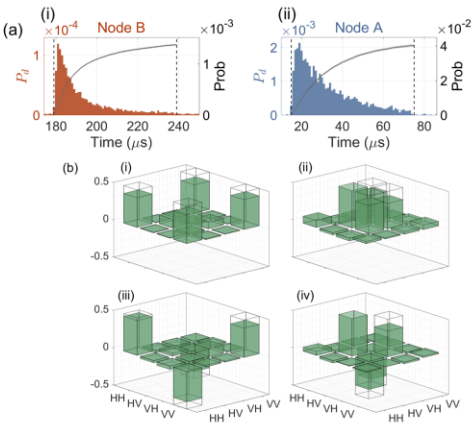

FIG. 5. **Repeater node protocol results.** (a) Left axes: probability distribution (P_d) for single-photon detection per 1 µs time bin. Time origins: Raman laser pulse onset. Dashed black lines: windows where DBSM is performed. Right axes: cumulative photon detection probability. (b) Colored bars show measured real parts of the density matrix of the two single-photon polarisation qubits shared by nodes A and B. Fidelities with targeted Bell states (wire frame) are (i) 78^{+3}_{-3}%, (ii) 80^{+3}_{-4}%, (iii) 83^{+3}_{-4}%, (iv) 84^{+3}_{-3}%.

Protocol differences. The described protocol is not identical to the one described in the trapped-ion repeater node demonstration of [16]. In [16] a *symmetric* protocol was implemented, in which attempts to deliver photons to both nodes were made in the first loop: whichever ion-qubit succeeded in delivering its photon was then stored in memory and attempts to deliver the final photon from the other ion were made in the second loop. In that work, the detection probability was similar at the two remote nodes at around 1×10^{-3}. In the present network, the detection probabilities at the nodes are strongly asymmetric, with a significantly higher value at the local node. Running the symmetric protocol would therefore almost always lead to successful detection at the local node first and the need to store the qubit in memory until the remote node succeeds (the time required for an average

of 1×10^3 attempts). We therefore run an asymmetric protocol in the present work, which always attempts to deliver to the remote node first and the local node second, thereby strongly reducing the memory storage time at negligible cost to the overall success probability. Minimising the time spent in memory, and therefore the number of photon generation attempts in Loop 2, is beneficial not only due to the reduced decoherence of the memory but also because the expected photon generation efficiency in Loop 2 is lower than in Loop 1 due to the absence of optimal electronic state preparation (optical pumping).

Interleaved calibrations. Execution of the repeater protocol is interleaved with a variety of calibration measurements, including a total of five polarisation stabilisation runs, consecutively spaced by an average of 1.5 hours. The lowest fidelity between two consecutive fiber processes matrices was 0.96, revealing a slight but measurable drift in the Channel Q birefringence. A second interleaved calibration measurement is tomographic reconstruction of the distributed ion-photon states, which was also repeated a total of five times spaced by a similar average time. Here, the repeater protocol is executed with one modification: the MS gate is replaced with laser pulses enabling tomographic analysis of the established ion-photon states. Adding up all the data from those five repeated measurement sets yields two ion-photon states, one between ion 1 and the 1550 nm photonic polarisation qubit delivered remotely (ρ_{ip}^B), and one between ion 2 and the 854 nm photonic polarisation qubit delivered locally (ρ_{ip}^A). Those states represent our best estimates of the average distributed ion-photon states over the time period during which the full repeater node protocol was run, and already include imperfections due to e.g., the aforementioned channel birefringence changes. Additional interleaved calibration measurements are described in Appendix A.III.3.

Probabilities and memory advantages. The repeater protocol was executed a total of 67000 times over 101.14 minutes, during which 4479061 attempts were made to establish photonic entanglement between nodes A and B, and 3369 successes occurred. The success probability is therefore $P_s = 7.5(1) \times 10^{-4}$. Successes correspond to asynchronous detection of a photon at each node, where each photon is detected within a 60 μs-wide time window containing the single photon wavepackets (Figure 5(a)). The value of P_s can be compared with the expected probability P_s^{single} to establish Node A-B entanglement without exploiting the ion memory. We calculate $P_s^{single} = P_{B,1} \times P_{A,2} = 5.5(1) \cdot 10^{-5}$ where $P_{B,1} = 1.38(2) \cdot 10^{-3}$ and $P_{A,2} = 4.02(7) \cdot 10^{-2}$ are the measured probabilities for single photon detection at Nodes B and A, respectively. The ion memory thus enhances the success probability by a factor $\alpha = P_s/P_s^{single} = 13.6(3)$. In principle, by performing enough Loop-2 attempts, one can approach unit probability for the detection of the second photon yielding the maximum memory enhancement factor for our experiment of $\alpha^{max} = 1/P_{A,2} = 24.9(4)$. In the presented experiment, the 22 attempts in Loop 2 resulted in a total probability for detecting the second photon of 0.56(1) limiting α to be $\alpha = \alpha^{max} \times 0.56(1)$. Increasing the number of Loop-2 attempts could only thus increase the overall success probability by less than a factor of two. The measured wavepackets of photons produced from the ions are expected (and numerically predicted) to differ due to the absence of optimal electronic state preparation (optical pumping) on ion 2.

Photon-photon states. Figure 5(a) presents the four measured two-photon density matrices, reconstructed from the 3369 total successes, and each measured conditioned on a different logical output state of the ion-qubits. Each matrix has been rotated, from the one directly reconstructed, by the same two single-qubit rotations. Those local rotations, found by numerical search to maximise the average fidelities with Bell states, do not change the entanglement content of the four states, nor their inner products, and bring the measured states into the familiar Bell state form. We attribute these rotations to the polarisation rotations imparted by the different optical fiber paths to the two analysis stations. The concurrences and Bell state fidelities of the measured states are $[59^{+8}_{-5}, 63^{+6}_{-7}, 72^{+6}_{-8}, 71^{+6}_{-6}]$ and $[78^{+3}_{-3}, 80^{+3}_{-4}, 83^{+3}_{-4}, 84^{+3}_{-3}]\%$, respectively, proving clearly entangled states.

Using the data underlying all four photon-photon states, a numerical calculation is performed to simulate the process known as feedforward, in which the photon states are further locally rotated (conditional on the ion outcome) such that the repeater always delivers a single Bell-like state to the remote nodes. The obtained state ρ_{pp}^{ff} has a Bell state fidelity of $82^{+2}_{-1}\%$, respectively, as detailed in Appendix A.III.5. Our repeater protocol thus succeeds in establishing entanglement between photons detected at the two remote analysis stations.

Protocol fidelity limits. To identify the origins of protocol infidelity we develop a model of the distributed photon-photon state ρ_{pp}^{ff}. The model takes as input the measured distributed ion-photon states ρ_{ip}^B and ρ_{ip}^A obtained during the interleaved calibrations. Next, perfect DBSM and feedforward operations are applied numerically to those states, yielding a single predicted photon-photon Bell-like state. The model predicts a photon-photon Bell state fidelity of $82^{+2}_{-2}\%$, which is statistically consistent with the measured value of $82^{+2}_{-1}\%$. Therefore, imperfections in the DBSM, due to e.g., an imperfect MS gate, are not resolved in the measured photon-photon state fidelity. Up to the statistical precision of our measurements, the infidelities in the measured photon-photon state ρ_{pp}^{ff} are already present in the ion-photon states ρ_{ip}^B and ρ_{ip}^A distributed in the repeater-node protocol. Those ion-photon states have fidelities with maximally-entangled states of 0.87(1) (photon sent to B) and 0.92(1) (photon send to A), respectively. The origins of infidelities in those ion-photon states are now discussed and more details can be found in Appendix A.III.6.

The ion-qubit in ρ_{ip}^B is stored in the ground state memory of ion 1 for up to 4.4 ms, during attempts to gener-

ate photons from the co-trapped ion in loop 2. We determine that an otherwise perfect ion-photon Bell state would have its fidelity reduced by 0.060(5) due to qubit storage in the ion 1 memory during the repeater protocol. That value is determined from a separate set of calibration measurements performed on the same day. This infidelity is expected to originate from frequency offsets between spin-echo pulses and the ground state qubit transition, due to ambient field fluctuations at the local powerline frequency of 50 Hz. Separately, the average detector background counts measured at Location B are expected to contribute a Bell-state infidelity of 0.07(1). The 0.13(1) infidelity in the measured ion-photon state ρ_{ip}^{B} is thus accounted for by detector darks counts and imperfect storage in the ion 1 memory. In upcoming work we show that the coherence time of our ion memories can be significantly extended beyond the performance reported here, in the presence of photon generation, using a more advanced dynamical decoupling sequence [53].

As previously stated, the ion-photon state ρ_{ip}^{A} involving ion 2 and an 854 nm photon detected at location A has a fidelity of 0.92(1). That state is not stored in memory and the relevant recorded detector background accounts for a fidelity drop of only 0.007(4). The state fidelity is several percent lower than the value achieved for a single trapped ion in the previous section and than we have previously achieved in comparable situations [16, 31, 54]. Moreover, when measured in the lab using the same photon detection path, the ion-photon Bell state generated from ion 2 was consistently of lower fidelity than the one generated by ion 1. We have not yet identified the origins of the missing fidelity involving the second ion. To within statistical precision, the Bell state fidelity of ρ_{ip}^{A} is limited by is purity and therefore error sources that result in non-unitary errors in the reconstructed ion-photon quantum state are at fault. One possibility is miscalibration of the laser pulses involved in the analysis of the ion-qubit encoded in ion 2.

III. CONCLUSION, DISCUSSION AND OUTLOOK

Yet to be written.

ACKNOWLEDGMENTS

Yet to be written.

AUTHOR CONTRIBUTION STATEMENT

Yet to be written.

[1] H. J. Kimble, *The quantum internet,* Nature **453**, 1023 (2008).
[2] Stephanie Wehner, David Elkouss, and Ronald Hanson, *Quantum internet: A vision for the road ahead,* Science **362**, eaam9288 (2018).
[3] Stefano Pirandola, Ulrik L. Andersen, Leonardo Banchi, Mario Berta, Darius Bunandar, Roger Colbeck, Dirk Englund, Tobias Gehring, Cosmo Lupo, Carlo Ottaviani, Jason L. Pereira, Mohsen Razavi, Jesni Shamsul Shaari, Marco Tomamichel, Vladyslav C. Usenko, Giuseppe Vallone, Paolo Villoresi, and Petros Wallden, *Advances in quantum cryptography,* Adv. Opt. Photon. **12**, 1012–1236 (2020), arXiv:1906.01645.
[4] Liang Jiang, J. M. Taylor, Anders S. Sørensen, and Mikhail D. Lukin, *Distributed quantum computation based on small quantum registers,* Physical Review A **76**, 062323 (2007).
[5] Zheshen Zhang and Quntao Zhuang, *Distributed quantum sensing,* Quantum Sci. Technol. **6**, 043001 (2021), arXiv:2010.14744.
[6] P. Kómár, E. M. Kessler, M. Bishof, L. Jiang, A. S. Sørensen, J. Ye, and M. D. Lukin, *A quantum network of clocks,* Nature Physics **10**, 582 (2014).
[7] Jelena V. Rakonjac, Samuele Grandi, Sören Wengerowsky, Dario Lago-Rivera, Félicien Appas, and Hugues de Riedmatten, *Transmission of light–matter entanglement over a metropolitan network,* Optica Quantum **1**, 94 (2023).
[8] Arian J. Stolk, Kian L. van der Enden, Marie-Christine Slater, Ingmar te Raa-Derckx, Pieter Botma, Joris van Rantwijk, J. J. Benjamin Biemond, Ronald A. J. Hagen, Rodolf W. Herfst, Wouter D. Koek, Adrianus J. H. Meskers, René Vollmer, Erwin J. van Zwet, Matthew Markham, Andrew M. Edmonds, J. Fabian Geus, Florian Elsen, Bernd Jungbluth, Constantin Haefner, Christoph Tresp, Jürgen Stuhler, Stephan Ritter, and Ronald Hanson, *Metropolitan-scale heralded entanglement of solid-state qubits,* Science Advances **10**, eadp6442 (2024).
[9] Eric Bersin, Matthew Grein, Madison Sutula, Ryan Murphy, Yan Qi Huan, Mark Stevens, Aziza Suleymanzade, Catherine Lee, Ralf Riedinger, David J. Starling, Pieter-Jan Stas, Can M. Knaut, Neil Sinclair, Daniel R. Assumpcao, Yan-Cheng Wei, Erik N. Knall, Bartholomeus Machielse, Denis D. Sukachev, David S. Levonian, Mihir K. Bhaskar, Marko Lončar, Scott Hamilton, Mikhail Lukin, Dirk Englund, and P. Benjamin Dixon, *Development of a boston-area 50-km fiber quantum network testbed,* Phys. Rev. Appl. **21**, 014024 (2024).
[10] Stephan Kucera, Christian Haen, Elena Arenskötter, Tobias Bauer, Jonas Meiers, Marlon Schäfer, Ross Boland, Milad Yahyapour, Maurice Lessing, Ronald Holzwarth, Christoph Becher, and Jürgen Eschner, *Demonstration of quantum network protocols over a 14-km urban fiber link,* npj Quantum Information **10**, 88 (2024).

[11] Jian-Long Liu, Xi-Yu Luo, Yong Yu, Chao-Yang Wang, Bin Wang, Yi Hu, Jun Li, Ming-Yang Zheng, Bo Yao, Zi Yan, Da Teng, Jin-Wei Jiang, Xiao-Bing Liu, Xiu-Ping Xie, Jun Zhang, Qing-He Mao, Xiao Jiang, Qiang Zhang, Xiao-Hui Bao, and Jian-Wei Pan, *Creation of memory–memory entanglement in a metropolitan quantum network,* Nature **629**, 579 (2024).

[12] Wolfgang Dür, Hans J. Briegel, Juan Ignacio Cirac, and Peter Zoller, *Quantum repeaters based on entanglement purification,* Phys. Rev. A **59**, 169 (1999), arXiv:quant-ph/9808065.

[13] Zhen-Sheng Yuan, Yu-Ao Chen, Bo Zhao, Shuai Chen, Jörg Schmiedmayer, and Jian-Wei Pan, *Experimental demonstration of a bdcz quantum repeater node,* Nature **454**, 1098 (2008).

[14] N. Kalb, A. A. Reiserer, P. C. Humphreys, J. J. W. Bakermans, S. J. Kamerling, N. H. Nickerson, S. C. Benjamin, D. J. Twitchen, M. Markham, and R. Hanson, *Entanglement distillation between solid-state quantum network nodes,* Science **356**, 928 (2017), https://www.science.org/doi/pdf/10.1126/science.aan0070.

[15] S. Langenfeld, P. Thomas, O. Morin, and G. Rempe, *Quantum repeater node demonstrating unconditionally secure key distribution,* Phys. Rev. Lett. **126**, 230506 (2021).

[16] V. Krutyanskiy, M. Canteri, M. Meraner, J. Bate, V. Krcmarsky, J. Schupp, N. Sangouard, and B. P. Lanyon, *Telecom-wavelength quantum repeater node based on a trapped-ion processor,* Phys. Rev. Lett. **130**, 213601 (2023).

[17] Juan Ignacio Cirac and Peter Zoller, *Quantum Computations with Cold Trapped Ions,* Phys. Rev. Lett. **74**, 4091–4094 (1995).

[18] L.-M. Duan and C. Monroe, *Colloquium: Quantum networks with trapped ions,* Rev. Mod. Phys. **82**, 1209 (2010).

[19] Andreas Stute, Bernardo Casabone, Philipp Schindler, Thomas Monz, Piet O. Schmidt, Birgit Brandstätter, Tracy E. Northup, and Rainer Blatt, *Tunable ion-photon entanglement in an optical cavity,* Nature **485**, 482 (2012), arXiv:1301.0275.

[20] D. L. Moehring, P. Maunz, S. Olmschenk, K. C. Younge, D. N. Matsukevich, L.-M. Duan, and C. Monroe, *Entanglement of single-atom quantum bits at a distance,* Nature **449**, 68 (2007).

[21] D. Hucul, I. V. Inlek, G. Vittorini, C. Crocker, S. Debnath, S. M. Clark, and C. Monroe, *Modular entanglement of atomic qubits using photons and phonons,* Nature Physics **11**, 37 (2014).

[22] Laurent J. Stephenson, David P. Nadlinger, Bethan C. Nichol, Shuoming An, Peter Drmota, Timothy G. Ballance, Keshav Thirumalai, Joseph F. Goodwin, David M. Lucas, and Christopher J. Ballance, *High-Rate, High-Fidelity Entanglement of Qubits Across an Elementary Quantum Network,* Phys. Rev. Lett. **124**, 110501 (2020), arXiv:1911.10841.

[23] Victor Krutyanskiy, Maria Galli, Vojtech Krcmarsky, Simon Baier, Dario Alessandro Fioretto, Yunfei Pu, Azadeh Mazloom, Pavel Sekatski, Marco Canteri, Markus Teller, Josef Schupp, James Bate, Martin Meraner, Nicolas Sangouard, Ben P. Lanyon, and Tracy E. Northup, *Entanglement of Trapped-Ion Qubits Separated by 230 Meters,* Phys. Rev. Lett. **130**, 050803 (2023), arXiv:2208.14907.

[24] Z. B. Cui, Z. Q. Wang, P. C. Lai, Y. Wang, J. X. Shi, P. Y. Liu, Y. D. Sun, Z. C. Tian, Y. B. Liang, B. X. Qi, Y. Y. Huang, Z. C. Zhou, Y. K. Wu, Y. Xu, L. M. Duan, and Y. F. Pu, *A metropolitan-scale trapped-ion quantum network node with hybrid multiplexing enhancements,* arXiv:2503.13898 [quant-ph] (2025).

[25] C. Monroe, R. Raussendorf, A. Ruthven, K. R. Brown, P. Maunz, L.-M. Duan, and J. Kim, *Large-scale modular quantum-computer architecture with atomic memory and photonic interconnects,* Phys. Rev. A **89**, 022317 (2014).

[26] Bethan C. Nichol, Raghavendra Srinivas, David P. Nadlinger, Peter Drmota, Dougal Main, Gabriel Araneda, Christopher J. Ballance, and David M. Lucas, *An elementary quantum network of entangled optical atomic clocks,* Nature **609**, 689 (2022), arXiv:2111.10336.

[27] Dougal Main, Peter Drmota, David P. Nadlinger, Ellis M. Ainley, Ayush Agrawal, Bethan C. Nichol, Raghavendra Srinivas, Gabriel Araneda, and David M. Lucas, *Distributed quantum computing across an optical network link,* Nature **638**, 383 (2025), arXiv:2407.00835.

[28] Wen-Zhao Liu, Ya-Bin Zhou, Jiu-Peng Chen, Bin Wang, Ao Teng, Xiao-Wen Han, Guang-Cheng Liu, Zhi-Jiong Zhang, Yi Yang, Feng-Guang Liu, Chao-Hui Xue, Bo-Wen Yang, Jin Yang, Chao Zeng, Du-Ruo Pan, Ming-Yang Zheng, Xingjian Zhang, Shen Cao, Yi-Zheng Zhen, You Xiao, Hao Li, Lixing You, Xiongfeng Ma, Qi Zhao, Feihu Xu, Ye Wang, Yong Wan, Qiang Zhang, and Jian-Wei Pan, *Long-lived remote ion-ion entanglement for scalable quantum repeaters,* Nature (2026), 10.1038/s41586-026-10177-4.

[29] Matthias Bock, Pascal Eich, Stephan Kucera, Matthias Kreis, Andreas Lenhard, Christoph Becher, and Jürgen Eschner, *High-fidelity entanglement between a trapped ion and a telecom photon via quantum frequency conversion,* Nature Communications **9**, 1998 (2018).

[30] Victor Krutyanskiy, Martin Meraner, Josef Schupp, Vojtech Krcmarsky, H. Hainzer, and Ben P. Lanyon, *Light-matter entanglement over 50 km of optical fibre,* npj Quantum Inf. **5**, 72 (2019), arXiv:1901.06317.

[31] Victor Krutyanskiy, Marco Canteri, Martin Meraner, Vojtech Krcmarsky, and Ben P. Lanyon, *Multimode Ion-Photon Entanglement over 101 Kilometers,* PRX Quantum **5**, 020308 (2024), arXiv:2308.08891.

[32] Koji Azuma, Sophia E. Economou, David Elkouss, Paul Hilaire, Liang Jiang, Hoi-Kwong Lo, and Ilan Tzitrin, *Quantum repeaters: From quantum networks to the quantum internet,* Rev. Mod. Phys. **95**, 045006 (2023), arXiv:2212.10820.

[33] Max Bergerhoff, Omar Elshehy, Stephan Kucera, Matthias Kreis, and Jürgen Eschner, *Quantum repeater node with free-space coupled trapped ions,* Phys. Rev. A **110**, 032603 (2024), arXiv:2312.14805.

[34] Open Government Data Österreich-CC BY 4.0, *https://basemap.at/,* Accessed January 14, 2026.

[35] QGIS Development Team, *https://www.qgis.org,* Accessed January 14, 2026.

[36] Mika A. Zalewski, Denton Wu, Ana Luiza Ferrari, Yuanheng Xie, and Norbert M. Linke, *Kilometer-scale ion-photon entanglement with a metastable $^{88}Sr^{+}$ qubit,* Phys. Rev. A **113**, 012615 (2026).

[37] Marco Canteri, Zhe Xian Koong, James Bate, Armin Winkler, Victor Krutyanskiy, and Ben P. Lanyon, *Photon-Interfaced Ten-Qubit Register of Trapped Ions,*

Phys. Rev. Lett. **135**, 080801 (2025).
[38] A. Stute, B. Casabone, P. Schindler, T. Monz, P. O. Schmidt, B. Brandstätter, T. E. Northup, and R. Blatt, *Tunable ion-photon entanglement in an optical cavity,* Nature **485**, 482 (2012).
[39] Anders Sørensen and Klaus Mølmer, *Quantum computation with ions in thermal motion,* Phys. Rev. Lett. **82**, 1971 (1999).
[40] Zentralanstalt für Meteorologie und Geodynamik (ZAMG) and Department of Atmospheric and Cryospheric Sciences (ACINN), Universität Innsbruck, *ACInn station portal: download meteorological raw data,* Accessed January 14, 2026.
[41] Michael A. Nielsen and Isaac L. Chuang, *Quantum Computation and Quantum Information*, 10th Anniversary Edition ed. (Cambridge University Press, Cambridge, U.K., 2010).
[42] Alexander Treiber, Andreas Poppe, Michael Hentschel, Daniele Ferrini, Thomas Lorünser, Edwin Querasser, Thomas Matyus, Hannes Hübel, and Anton Zeilinger, *A fully automated entanglement-based quantum cryptography system for telecom fiber networks,* New Journal of Physics **11**, 045013 (2009).
[43] Sebastian Philipp Neumann, Alexander Buchner, Lukas Bulla, Martin Bohmann, and Rupert Ursin, *Continuous entanglement distribution over a transnational 248 km fiber link,* Nature Communications **13**, 6134 (2022).
[44] Tim Strobel, Michal Vyvlecka, Ilenia Neureuther, Tobias Bauer, Marlon Schäfer, Stefan Kazmaier, Nand Lal Sharma, Raphael Joos, Jonas H. Weber, Cornelius Nawrath, Weijie Nie, Ghata Bhayani, Caspar Hopfmann, Christoph Becher, Peter Michler, and Simone Luca Portalupi, *Quantum teleportation with telecom photons from remote quantum emitters,* arXiv:2411.12904 (2024).
[45] Alexander N. Craddock, Anne Lazenby, Gabriel Bello Portmann, Rourke Sekelsky, Mael Flament, and Mehdi Namazi, *Automated distribution of polarization-entangled photons using deployed new york city fibers,* PRX Quantum **5**, 030330 (2024).
[46] Scott Hill and William K. Wootters, *Entanglement of a Pair of Quantum Bits,* Phys. Rev. Lett. **78**, 5022–5025 (1997), arXiv:quant-ph/9703041.
[47] C. A. Sackett, D. Kielpinski, B. E. King, C. Langer, V. Meyer, C. J. Myatt, M. Rowe, Q. A. Turchette, W. M. Itano, D. J. Wineland, and C. Monroe, *Experimental entanglement of four particles,* Nature **404**, 256 (2000).
[48] B. Efron and R. Tibshirani, *Bootstrap methods for standard errors, confidence intervals, and other measures of statistical accuracy,* Statist. Sci. **1**, 54 (1986).
[49] Birgit Ursula Brandstätter, *Integration of fiber mirrors and ion traps for a high-fidelity quantum interface*, Ph.D. thesis, University of Innsbruck (2013).
[50] H.-J. Briegel, W. Dür, J. I. Cirac, and P. Zoller, *Quantum repeaters: The role of imperfect local operations in quantum communication,* Phys. Rev. Lett. **81**, 5932 (1998).
[51] Anders Sørensen and Klaus Mølmer, *Entanglement and quantum computation with ions in thermal motion,* Phys. Rev. A **62**, 022311 (2000).
[52] Jan Benhelm, Gerhard Kirchmair, Christian F. Roos, and Rainer Blatt, *Towards fault-tolerant quantum computing with trapped ions,* Nature Physics **4**, 463 (2008).
[53] James Bate, Johannes Helgert, Marco Canteri, , Victor Krutyanskiy, and Ben P. Lanyon, *A cavity-interfaced trapped-ion regiter with multi-second coherence,* (2026), in preparation.
[54] Marco Canteri, James Bate, Ida Mishra, Nicolai Friis, Victor Krutyanskiy, and Benjamin P. Lanyon, *Generation of multipartite photonic entanglement using a trapped-ion quantum processing node,* arXiv:ABCDE.XYZX [quant-ph] (2025).
[55] *Interface between trapped-ion qubits and travelling photons with close-to-optimal efficiency*, Ph.D. thesis, University of Innsbruck (2021).
[56] Josef Schupp, Vojtech Krcmarsky, Victor Krutyanskiy, Martin Meraner, Tracy E. Northup, and Ben P. Lanyon, *Interface between Trapped-Ion Qubits and Traveling Photons with Close-to-Optimal Efficiency,* PRX Quantum **2**, 020331 (2021), arXiv:2105.02121.
[57] Zdeněk Hradil, Jaroslav Řeháček, Jaromír Fiurášek, and Miroslav Ježek, *Maximum-likelihood methods in quantum mechanics,* in *Quantum State Estimation*, Lecture Notes in Physics, Vol. 649 (Springer, 2004) pp. 59–112.
[58] Dario Alessandro Fioretto, *Towards a flexible source for indistinguishable photons based on trapped ions and cavities*, Ph.D. thesis, University of Innsbruck (2020).
[59] Cornelius Hempel, *Digital quantum simulation, Schrödinger cat state spectroscopy and setting up a linear ion trap*, Ph.D. thesis, University of Innsbruck (2014).
[60] Gerhard Kirchmair, *Quantum non-demolition measurements and quantum simulation*, Ph.D. thesis, University of Innsbruck (2010)

Appendix C – Bibliography

[Bate25] J. Bate, A. Hamann, M. Canteri, A. Winkler, Z. Koong, V. Krutyanskiy, W. Dür, and B.P. Lanyon, Experimental distributed quantum sensing in a noisy environment, Phys. Rev. Lett. 135, 220801 (2025)

[Bate26] Bate, James and Helgert, Johannes and Canteri, Marco and and Krutyanskiy, Victor and Lanyon, Ben P. 'A Cavity-Interfaced Trapped-Ion regiter with Multi-Second Coherence', in preparation (2026).

[Berg24] Max Bergerhoff, Omar Elshehy, Stephan Kucera, Matthias Kreis, and Jürgen Eschner, Quantum repeater node with free-space coupled trapped ions, Phys. Rev. A 110, 032603 (2024)

[Cant25a] M. Canteri, Z. Koong, J. Bate, A. Winkler, V. Krutyanskiy, and B.P. Lanyon, A photon-interfaced ten qubit quantum network node, Phys. Rev. Lett. 135, 080801 (2025) - see also press release and Physics World article

[Cant25b] M Canteri, J Bate, I Mishra, N Friis, V Krutyanskiy, BP Lanyon, Generation of multipartite photonic entanglement using a trapped-ion quantum processing node, Preprint arXiv:2510.15693 (2025)

[Helg24] Johannes Helgert, Radio frequency control of a trapped-ion quantum network node, Master thesis, University of Innsbruck, 2024. See https://www.uibk.ac.at/en/exphys/research/dqs/publications/

[Rung25] Tatjana Runggaldier, Ion-photon entanglement over a 17 km-long optical fibre deployed across Innsbruck, Master thesis, University of Innsbruck, 2025. See https://www.uibk.ac.at/en/exphys/research/dqs/publications/

[Kodok26] F. Kodokkat, T. Runggaldier, A. Winkler, F. Bernecker, J. Bate, M. Canteri, J. Helgert, T. E. Northup, V. Krutyanskiy, and B. P. Lanyon, Trapped-ion based quantum repeater node across a 17 km-long metropolitan fiber, in preparation (2026)

[Krut19] V. Krutyanskiy, M. Meraner, J. Schupp, V. Krcmarsky, H. Hainzer & B. P. Lanyon, Light-matter entanglement over 50 km of optical fibre, npj Quantum Inf 5, 72 (2019)

[Krut23a] V. Krutyanskiy, M. Canteri, M. Meraner, J. Bate, V. Krcmarsky, J. Schupp, N. Sangouard, B. P. Lanyon, A telecom wavelength quantum repeater node based on a trapped-ion processor, Phys. Rev. Lett. 130, 213601 (2023) - see also Physics World reveals its top 10 Breakthroughs of the Year for 2023

[Krut23b] V. Krutyanskiy, M. Galli, V. Krcmarsky, S. Baier, D. A. Fioretto, Y. Pu, A. Mazloom, P. Sekatski, M. Canteri, M. Teller, J. Schupp, J. Bate, M. Meraner, N. Sangouard, B. P. Lanyon, T. E. Northup, Entanglement of trapped-ion qubits separated by 230 meters, Phys. Rev. Lett. 130, 050803 (2023) - see also press release and editors choice

[Krut24a] V. Krutyanskiy, M. Canteri, M. Meraner, V. Krcmarsky, and B.P. Lanyon, Multimode Ion-Photon Entanglement over 101 Kilometers, PRX Quantum 5, 020308 (2024)

[OPG] Open Government Data Osterreich-CC BY 4.0, https://basemap.at/, Accessed January 14, 2026.

[QGIS] QGIS Development Team, https://www.qgis.org, Accessed January 14, 2026.

[Stute12] A. Stute, B. Casabone, P. Schindler, T. Monz, P. O.Schmidt, B. Brandstätter, T. E. Northup, and R. Blatt, Tunable ion–photon entanglement in an optical cavity, Nature 485, 482 (2012).